Received: 11 October 2018 | Revised: 9 January 2019 | Accepted: 10 January 2019

DOI: 10.1002/nbm.4074

RESEARCH ARTICLE

WILEY NMR IN BIOMEDICINE

Diffusion-weighted MRI of the prostate without susceptibility artifacts: Undersampled multi-shot turbo-STEAM with rotated radial trajectories

Andreas Merrem[1] | Sabine Hofer[1] | Ali Seif Amir Hosseini[2] | Dirk Voit[1] | Klaus-Dietmar Merboldt[1] | Zhengguo Tan[1] | Jens Frahm[1]

[1] Biomedizinische NMR, Max-Planck-Institut für biophysikalische Chemie, Göttingen, Germany

[2] Department of Diagnostic and Interventional Radiology, University Medical Center Göttingen, Germany

Correspondence
Dr A. Merrem, Biomedizinische NMR, Max-Planck-Institut für biophysikalische Chemie, 37070 Göttingen, Germany.
Email: amerrem@gwdg.de

Funding information
Deutsche Krebshilfe e.V.

The aim of this study was to develop and evaluate a clinically feasible approach to diffusion-weighted (DW) MRI of the prostate without susceptibility-induced artifacts. The proposed method relies on an undersampled multi-shot DW turbo-STEAM sequence with rotated radial trajectories and a multi-step inverse reconstruction with denoised multi-shot phase maps. The total acquisition time was below 6 min for a resolution of 1.4 × 1.4 × 3.5 mm^3 and six directions at b = 600 s mm^{-2}. Studies of eight healthy subjects and two patients with prostate cancer were performed at 3 T employing an 18-channel body-array coil and elements of the spine coil. The method was compared with conventional DW echo-planar imaging (EPI) of the prostate. The results confirm that DW STEAM MRI avoids geometric distortions and false image intensities, which were present for both single-shot EPI (ssEPI) and readout-segmented EPI, particularly near the intestinal wall of the prostate. Quantitative accuracy of the apparent diffusion coefficient (ADC) was validated with use of a numerical phantom providing ground truth. ADC values in the central prostate gland of healthy subjects were consistent with those measured using ssEPI and with literature data. Preliminary results for patients with prostate cancer revealed a correct anatomical localization of lesions with respect to T_2-weighted MRI in both mean DW STEAM images and ADC maps. In summary, DW STEAM MRI of the prostate offers clinically relevant advantages for the diagnosis of prostate cancer compared with state-of-the-art EPI-based approaches. The method warrants extended clinical trials.

KEYWORDS

Cancer, diffusion-weighted MRI, iterative reconstruction, prostate, radial sampling

1 | INTRODUCTION

Prostate cancer is one of the most prevalent forms of cancer diagnosed in men worldwide.[1] A widely used tool for diagnosis and treatment monitoring is diffusion-weighted (DW) MRI,[2,3] a technique sensitive to tissue cellularity. Due to the anatomical location of the prostate, DW MRI faces two major challenges. First, if performed without an endorectal coil, the distance between the prostate and the imaging coils leads to a relatively low signal-to-noise

Abbreviations used: ADC, apparent diffusion coefficient; DW, diffusion weighted; EPI, echo-planar imaging; GPU, graphics processing unit; ROI, region of interest; rsEPI, readout-segmented EPI; SNR, signal-to-noise ratio; ssEPI, single-shot EPI; STEAM, stimulated echo acquisition mode.

ratio (SNR). Second, the position of the prostate and in particular its proximity to the often air-filled colon results in pronounced magnetic susceptibility differences and long-ranging variations of the magnetic field. This frequent problem causes geometric distortions as well as false image intensities in the most commonly used DW MRI technique, ie single-shot echo-planar imaging (ssEPI).[4] In fact, the inherent sensitivity of EPI to magnetic field inhomogeneities and susceptibility differences may seriously compromise diagnostic information in prostate MRI.[2,5] Although readout-segmented EPI (rsEPI) of the prostate has been shown to partly ameliorate the influence of susceptibility differences,[5] it may still lead to relevant image distortions.[6,7]

On the other hand, turbo-STEAM (stimulated echo acquisition mode) sequences[8,9] allow for DW MRI without any susceptibility-induced artifacts. They further avoid the high specific energy absorption rates of fast spin-echo sequences, which have also been proposed for DW MRI of the prostate.[10] However, a disadvantage of stimulated echoes is that they exploit only half of the signal strength of a corresponding spin-echo signal. To compensate for this deficiency, recent developments of DW STEAM MRI techniques took advantage of lessons learned from real-time MRI at high temporal resolution.[11] In this sense, single-shot DW STEAM sequences were improved with use of a highly undersampled radial acquisition scheme and image reconstruction by regularized nonlinear inversion to achieve artifact-free whole-brain DW MRI within measuring times of 1.5 to 2.5 min.[12] The resulting increase in signal strength stems from data undersampling, which leads to fewer stimulated echoes with correspondingly higher flip angles, and further benefits from reduced T_1 attenuation because of a shorter STEAM readout period. Moreover, the image intensities of an iteratively optimized numerical estimate no longer scale with the square root of the number of k-space acquisitions as known for Fourier transform MRI, which turns out to be especially advantageous for highly undersampled acquisitions. The underlying increase in SNR compared with preceding STEAM MRI variants[8,9] expands the range of possible applications and renders the technique a natural candidate for prostate imaging.

This work presents the development and first application of a novel turbo-STEAM method for DW MRI of the prostate. The lower SNR in comparison with brain studies required two major steps. First, the proposed method adopts a multi-shot acquisition scheme with rotated radial trajectories. Second, it uses a multi-step reconstruction scheme with nonlinear inverse estimation of coil sensitivities and denoising of phase maps from multiple shots with different sets of spokes. The final DW images are obtained by an iterative inverse optimization taking all shots into account. Accurate determinations of the apparent diffusion coefficient (ADC) were validated with use of a numerical phantom providing ground truth without suffering from potential experimental inadequacies. The feasibility and performance of the method was evaluated for a clinical setting at b-value 600 s mm^{-2} and the results were compared with state-of-the-art EPI-based protocols for DW MRI of the prostate. This pilot study included eight normal subjects and two patients.

2 | METHODS

2.1 | MRI

All studies were performed at 3 T using an MRI system with 80 mT m^{-1} gradients (Magnetom Prisma, Siemens Healthineers, Erlangen, Germany). DW turbo-STEAM MRI of the entire prostate was performed on eight young subjects without known illness using the 18-channel body-array coil and suitable elements of the spine coil. Preliminary clinical trials included two patients with elevated prostate-specific antigen (PSA) > 10 ng mL^{-1}. Prior to this study, both patients received standard multi-parametric MRI indicating a lesion in the transition zone with a Prostate Imaging Reporting and Data System Version 2 (PI-RADS v2) score of 5 in Patient 1 and two lesions in the transition zone with PI-RADS score of 5 in Patient 2. In all cases, written informed consent, according to the recommendations of the local ethics committee, was obtained prior to MRI.

A DW turbo-STEAM sequence with radial undersampling was implemented as recently described.[12] In order to improve the SNR and reconstruction stability for prostate imaging, this single-shot version was turned into a multi-shot acquisition with undersampled trajectories comprising 21 radial spokes which cover 360° of k-space. These trajectories were rotated from shot to shot in such a way as to equally fill the gaps between neighboring spokes (see Figure 1). The development of a suitable reconstruction technique is described in the next section. Fat suppression was achieved using a chemical-shift-selective pulse[13] before the acquisition of each shot. To cover the entire prostate, multiple slices without gaps were acquired in an interleaved order. Prior to the acquisition of DW images, five repetitions of the sequence were executed with b = 0 s mm^{-2} to achieve a steady state with respect to T_1 relaxation. The resulting images were used for an estimation of coil sensitivities. This step was followed by the acquisition of multi-shot DW MRI data for six diffusion gradient directions with b = 50 s mm^{-2} (three shots) and b = 600 s mm^{-2} (nine shots), respectively. Image resolution, field of view, and volume coverage were adapted to standard clinical protocols based on DW ssEPI and rsEPI as provided by the vendor. The parameters for all three protocols are summarized in Table 1. A few additional trials involved an experimental DW-STEAM MRI protocol with b-values of 50, 400, 800, and 1400 s mm^{-2} at a prolonged measuring time of about 20 min.

2.2 | Image reconstruction

Pre-processing of the DW multi-coil data comprised data compression by a principal component analysis, gradient delay correction, and interpolation onto a Cartesian grid. This was followed by an estimation of the coil sensitivities using a regularized nonlinear inverse reconstruction algorithm.[9] The development of a reconstruction process for multi-shot DW images with rotated k-space data involved the following steps. First, an image I_m for each shot was reconstructed using a linear inversion with L_2-regularization. These results were used to obtain denoised phase maps as given by

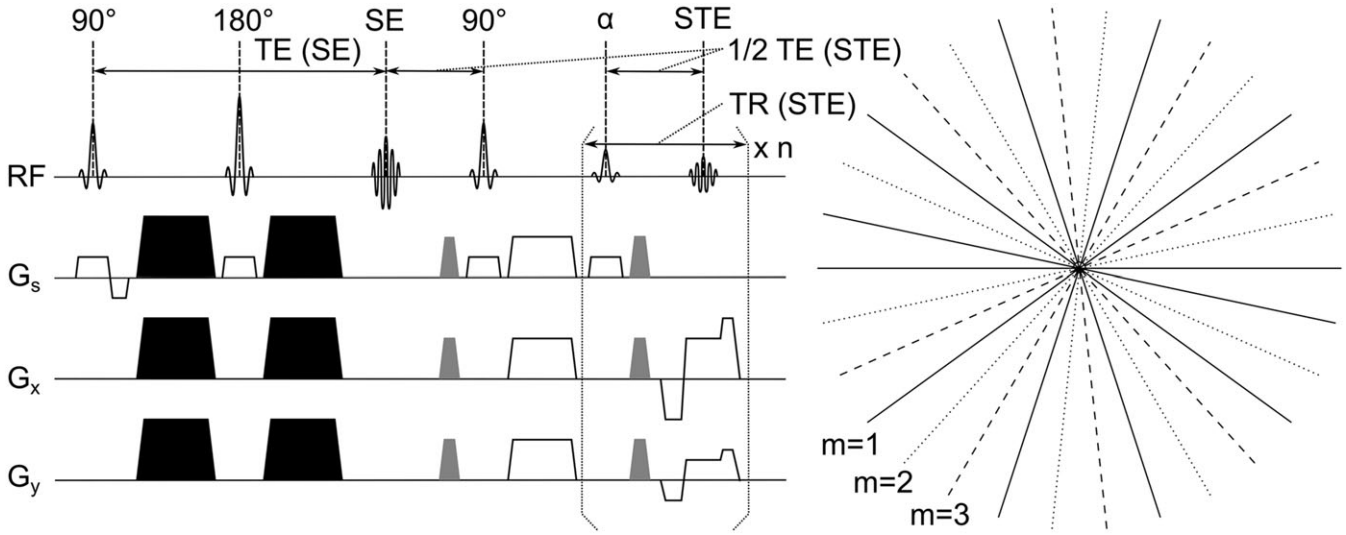

FIGURE 1 Left, DW STEAM MRI sequence; right, *k*-space trajectory for $m = 3$ shots. Black, diffusion gradients; gray, spoiler gradients; G_s, slice-selection gradient; G_x, G_y, frequency-encoding gradients; SE, spin echo; STE, stimulated echo; TE (SE), spin-echo time; TE (STE), stimulated echo time; TR (STE), repetition time of the STEAM readout sequence

TABLE 1 DW STEAM MRI, ssEPI and rsEPI of the prostate

	STEAM	ssEPI	rsEPI
Field of view/mm^2	200 × 200	200 × 200	200 × 200
Image matrix size	140 × 140	140 × 140	140 × 140
In-plane resolution/mm^2	1.43 × 1.43	1.43 × 1.43	1.43 × 1.43
Slice thickness/mm	3.5	3.5	3.5
Number of slices	21	21	21
TR/ms[a]	4582	3200	5300
TE (SE)/ms[b]	30.8	57	67
TR (STE)/ms[c]	7.61	–	–
TE (STE)/ms[d]	8.80	–	–
Bandwidth/Hz pixel^{-1}	200	1700	776
Partial Fourier factor	–	7/8	–
Segments	–	–	7
Diffusion gradient directions	6	6	3
b/s mm^{-2}	50, 600	50, 600	50, 600
Number of averages[e]	3, 9	4, 12	1, 3
Acquisition time/min: s[f]	5: 54	5: 25	7: 37

[a]Repetition time.

[b]Spin-echo time for $b = 600$ s mm^{-2}.

[c]STEAM repetition time.

[d]Stimulated-echo time.

[e]These numbers are shown in the same order as the *b*-values to which they refer.

[f]Total measurement time for multi-slice DW MRI and six diffusion gradient orientations.

$$e^{i\varphi_m} = \frac{\mathrm{NLM}(I_m)}{|\mathrm{NLM}(I_m)|}$$

where NLM denotes the application of a modified non-local means filter.[14] These phase maps were then used together with all coil sensitivities to reconstruct the image content r from all shots by minimizing the following cost function using the iteratively regularized Gauss-Newton algorithm:

$$\sum_{m,n} \left\| Y_{m,n} - P_m F\left(C_n e^{i\varphi_m} r\right) \right\|_2^2 + \alpha \|r\|_2^2.$$

C_n denotes the pre-calculated coil sensitivity profile for the nth virtual channel, $Y_{m,n}$ denotes the raw data for the mth shot and the nth virtual channel, and P_m denotes the projection on the k-space trajectory for the mth shot. Post-processing included denoising of the resulting images r with a modified non-local means filter[14] as well as computation of trace-weighted images and ADC maps as previously described for DW STEAM MRI of the brain.[12]

At this stage all reconstructions were performed offline. The algorithm was implemented on a single graphics processing unit (GPU), GeForce GTX TITAN (NVIDIA, Santa Clara, CA, USA) using the MATLAB Parallel Computing Toolbox (R2015b, MathWorks, Natick, MA, USA). To save memory on the GPU device, the coil sensitivity estimation was restricted to subsets of eight slices each instead of using the entire dataset. Total reconstruction time for a dataset of 21 slices for the entire prostate was approximately 2 h.

2.3 | Validation

The accuracy of ADC determinations was assessed with use of a numerical phantom (Figure 2) comprising multiple disjoint ellipses with defined ADC values between 0.8 and 2.2 × 10^{-3} mm^2 s^{-1} (ground truth). It refers to the generation of a set of raw data, ie the k-space data of the phantom, which can be computed by summation of the analytical Fourier transformation of used shapes such as ellipses or rectangles (see, eg, Block and Frahm[15]). Multi-coil parallel MRI was simulated by 30 receive coil sensitivities, which were generated via the sinusoidal approximation of spatially varying coil sensitivities. These sinusoidal coefficients can be integrated into the analytical Fourier transformation as described by Guerkin-Kern et al.[16]

The simulations employed the same radial trajectory (ie, 21 radial spokes rotated for multiple shots) and imaging parameters as chosen for the experimental STEAM protocol for DW MRI of the prostate (see Table 1): six diffusion directions, three shots with b = 50 s mm^{-2} and nine shots

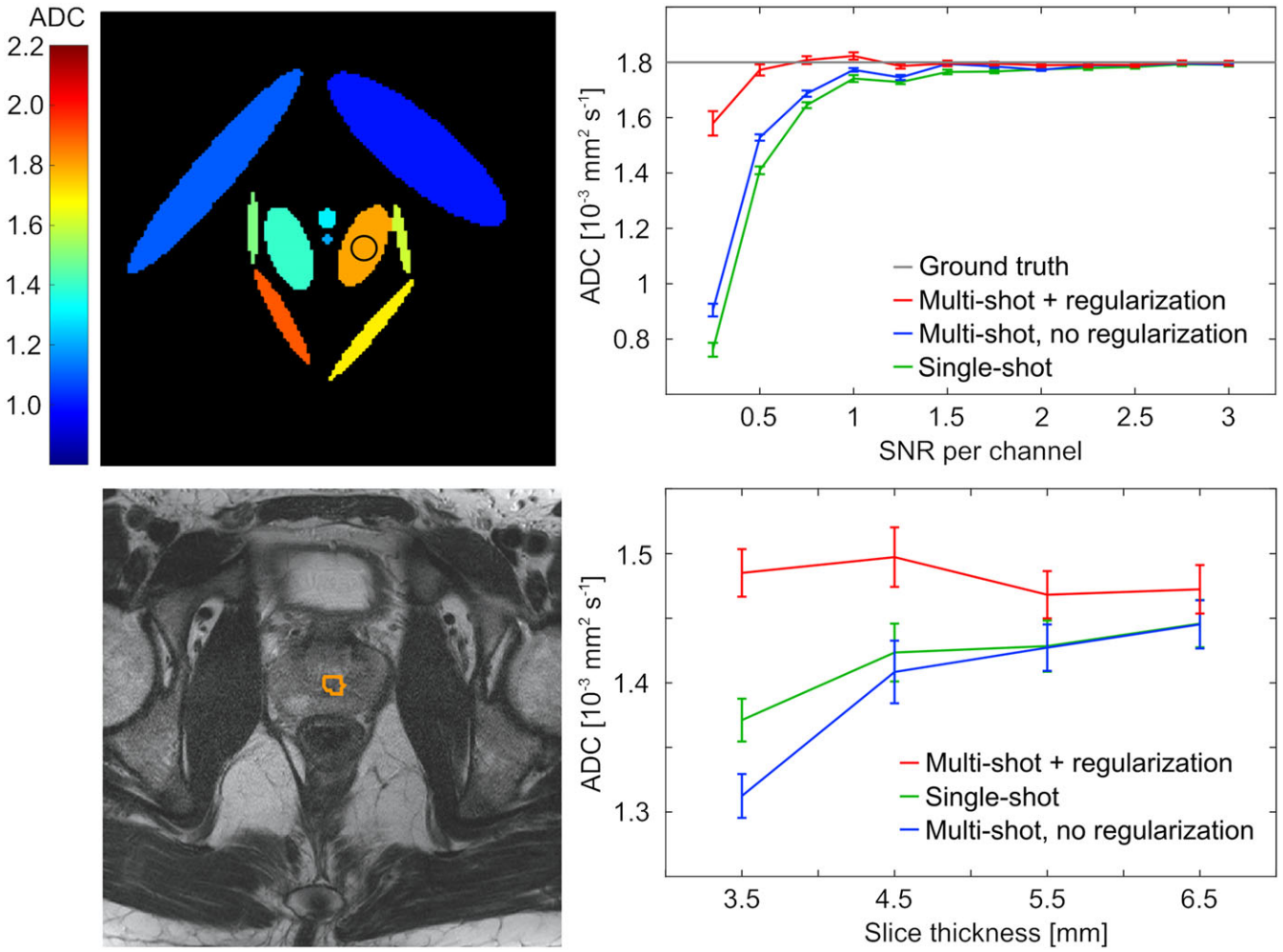

FIGURE 2 ADC as a function of SNR for a numerical phantom (top) and normal subjects (bottom). Upper left, numerical ADC map (ground truth) with circular ROI; upper right, corresponding values as a function of SNR for single-shot reconstructions with magnitude averaging[9] ("single-shot"), multi-shot reconstructions without phase map denoising[13] ("Multi-shot, no regularization"), and multi-shot reconstructions with denoised phase maps ("Multi-shot + regularization"). Lower left, T_2-weighted image with ROI in the central gland; lower right, corresponding ADC values as a function of slice thickness and reconstruction method. For details see text

with b = 600 s mm^{-2}. For b = 50 s mm^{-2} the intensity of all ellipses was set to 1, so that for b = 600 s mm^{-2} they are given by $I = e^{-550\ ADC}$ with the ADC in units of mm^2 s^{-1}. The phase was spatially homogeneous within each ellipse, but received a random value for each ellipse, shot, diffusion direction, and b-value to model unpredictable phase inconsistencies due to bulk tissue motion. The intensity outside the ellipses was set to zero. Prior to image reconstruction, white Gaussian noise was added to the calculated raw data to test different SNR levels.

Because of the known sensitivity of DW MRI to SNR, particular emphasis was placed on assessing the quantitative robustness of the proposed method as a function of SNR. Three different algorithms were compared for SNR values of 0.25 to 3 per receive channel: (i) single-shot reconstruction with magnitude averaging, $r = NLM(\langle|I_m|\rangle)$, as developed for DW STEAM MRI of the brain[12]; (ii) multi-shot reconstruction as described here but without denoising of phase maps[17]; and (iii) multi-shot reconstruction with denoised phase maps. The ADC was evaluated in a region of interest (ROI) and compared with ground truth.

To test the performance of the image reconstruction algorithm for the determination of in vivo prostate ADC values, DW STEAM MRI was obtained for different slice thicknesses between 3.5 and 6.5 mm (see Figure 2, bottom). ADC measurements were made in matched ROIs in the central gland of the prostate as covered in transverse sections which were centered at the same position. Further, the STEAM ADC values measured in an ROI of the central gland of all eight healthy volunteers were compared with those obtained in the same ROIs with DW ssEPI and rsEPI (see Table 2). Image reconstruction and post-processing of EPI-based acquisitions were performed using the online reconstruction software provided by the vendor.

Finally, the quality of the mean DW STEAM images and ADC maps of all eight subjects was assessed by an experienced abdominal and oncological radiologist (10 years of clinical practice) using a five-point Likert scale: 1, extremely poor, defined as "major artifacts, not clinically useful"; 2, poor, defined as "major artifacts, clinical use not advised"; 3, average, defined as "borderline clinical use"; 4, good, defined as "minor artifacts, not adversely affecting clinical use"; 5, excellent, defined as "no artifacts".

3 | RESULTS

The analysis of three different algorithms for DW STEAM MRI (Figure 2, top) demonstrates a superior performance of the proposed multi-shot reconstruction method with denoised phase maps. This particularly holds true for the case of low SNR, which affects the calculation of a quantitatively reliable ADC. In fact, ADC deviations from ground truth were less than twice the standard error of the regional mean for all simulations with an SNR higher than or equal to 0.5 per receive channel. In contrast, multi-shot reconstructions without phase denoising as well as single-shot reconstructions yielded ADC values significantly below the ground truth for SNR levels below 1.5 per receive channel.

When measuring ADC in the central gland of the prostate of healthy volunteers as a function of slice thickness (Figure 2, bottom), multi-shot reconstructions without phase map denoising and single-shot reconstructions were affected by decreasing ADC values for decreasing slice thickness. In contrast, for the proposed algorithm, the ADC was independent of slice thickness. This finding suggests that for the chosen experimental conditions the proposed reconstruction algorithm removes the systematic underestimation of the ADC, which is consistent with the numerical simulations for low SNR. Moreover, the measured ADC values are in agreement with literature values of (1.27 ± 0.14) × 10^{-3} mm^2 s^{-1} and (1.47 ± 0.24) × 10^{-3} mm^2 s^{-1}.[18,19] This also holds true for the mean prostate ADC value of (1.34 ± 0.09) × 10^{-3} mm^2 s^{-1} obtained for eight healthy volunteers (see Table 2). The difference between the mean ADC values measured with STEAM and ssEPI in these subjects was 1.19 times the standard error and therefore statistically not significant. On the other hand, marked differences between regional ADC values of individual subjects are likely to reflect inhomogeneity-induced signal variations in DW ssEPI. The ADC values measured with DW rsEPI were between 20% and 30% higher than those measured with the other two methods. These differences exceed their standard error by a factor greater than 5.

In all cases, DW STEAM images were in geometric correspondence to T_2-weighted spin-echo images, whereas EPI-based images showed visible distortions in 5/8 cases for ssEPI and in 4/8 cases for rsEPI. Most importantly, even in the vicinity of an air-filled colon (see Figure 3), the STEAM image

TABLE 2 ADC (10^{-3} mm^2 s^{-1}) in the central gland of the prostate

Subject	STEAM[a]	ssEPI[a]	rsEPI[a]
1	1.30 ± 0.10	1.14 ± 0.13	1.80 ± 0.21
2	1.39 ± 0.09	1.51 ± 0.16	1.64 ± 0.16
3	1.47 ± 0.13	1.50 ± 0.24	1.76 ± 0.24
4	1.27 ± 0.13	1.35 ± 0.22	1.65 ± 0.44
5	1.24 ± 0.12	1.33 ± 0.35	1.69 ± 0.31
6	1.34 ± 0.13	1.46 ± 0.26	1.69 ± 0.29
7	1.46 ± 0.13	1.61 ± 0.25	1.81 ± 0.29
8	1.31 ± 0.13	1.35 ± 0.15	1.74 ± 0.30
Mean ± SD[b]	1.34 ± 0.09	1.41 ± 0.14	1.72 ± 0.06

[a]Mean and standard deviation within the ROI.

[b]Mean and standard deviation of ADC values across subjects.

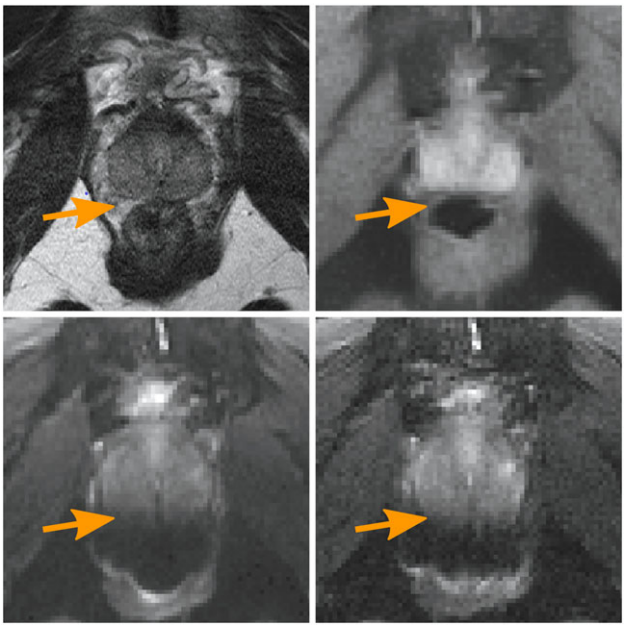

FIGURE 3 T_2-weighted image of the prostate of a healthy volunteer (upper left) and trace-weighted images (b = 50 s mm^{-2}) acquired with DW STEAM (upper right), DW ssEPI (lower left), and DW rsEPI (lower right). Only STEAM accurately depicts the anatomy near the intestinal wall, while ssEPI and rsEPI suffer from susceptibility-induced distortions (arrows)

offers an accurate anatomical representation of the prostate and intestinal wall. In contrast, both the ssEPI and rsEPI images show not only a distorted shape of the prostate, but also a severe degradation of image quality near the intestinal wall, which would compromise any diagnostic attempt. Moreover, EPI-based sequences yielded ADC maps with local hypointensities that were not present in ADC maps measured with DW STEAM MRI (see Figure 4). The radiological evaluation of the quality of mean DW images and ADC maps revealed acceptable image quality (ie, equal to 4 and 5 on the five-point Likert scale) in all eight cases, corresponding to images without artifacts or only minor artifacts that do not adversely affect the clinical use.

In the two patients studied here, all lesions detected by DW ssEPI could also be identified by DW STEAM MRI. In addition to adequate diffusion contrast and SNR, the STEAM images provide accurate anatomical information with respect to T_2-weighted MRI, which was partly corrupted in ssEPI results. For example, the STEAM ADC map for Patient 1 (see Figure 5) correctly localized the lesion at a distance of approximately 1 cm from the caudal boundary of the prostate, in agreement with the T_2-weighted image. Due to geometric distortions, this information is lost in the corresponding ssEPI ADC map. For Patient 2 (see Figure 6), the STEAM ADC map clearly delineates a lesion in the left transitional zone

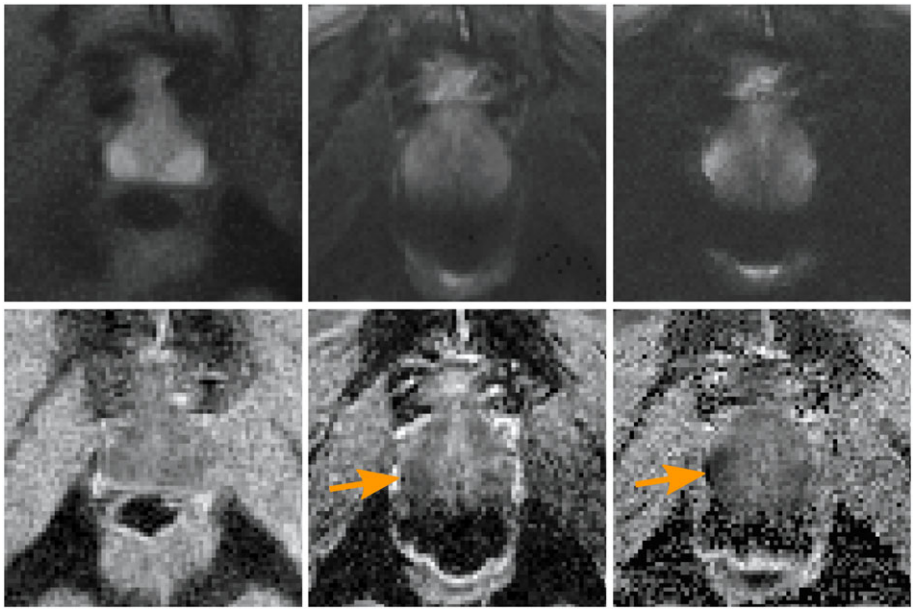

FIGURE 4 Trace-weighted images (b = 600 s mm^{-2}) (top) and ADC maps (bottom) of the same subject as in Figure 3 acquired with DW STEAM (left), DW ssEPI (middle), and DW rsEPI (right). The latter two show susceptibility-induced distortions (arrows)

FIGURE 5 DW MRI of patient 1 acquired with STEAM (top) and ssEPI (bottom). Left to right, T_2-weighted image, trace-weighted images at b = 50 s mm^{-2} and b = 600 s mm^{-2}, and ADC map. While the STEAM ADC map shows a lesion consistent with a low-signal area in the right transition zone in T_2-weighted MRI (PI-RADS score = 5), this lesion is less clear in the ssEPI ADC map (arrows)

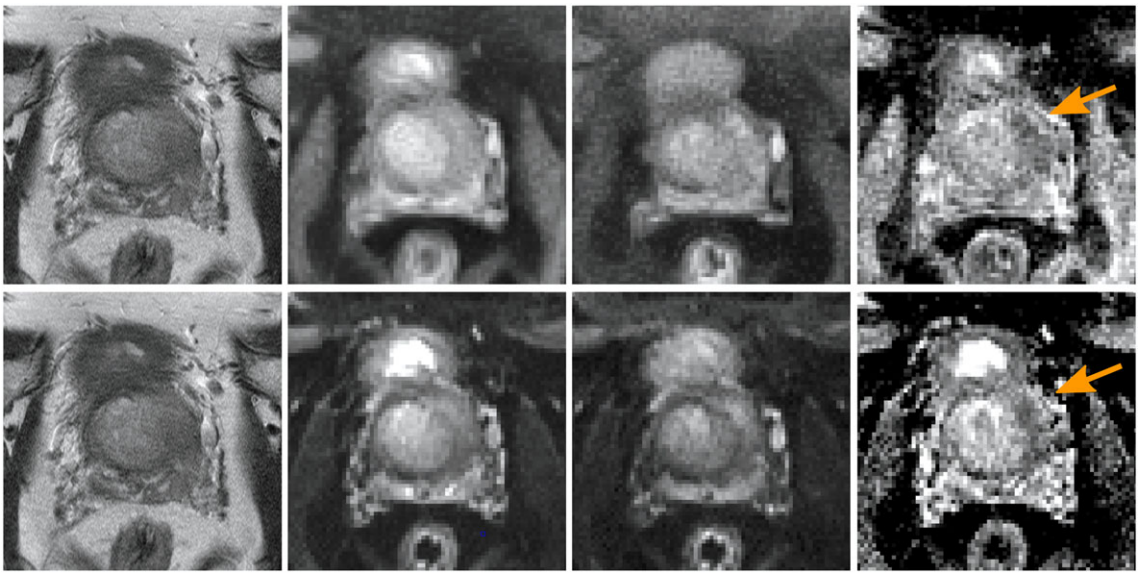

FIGURE 6 DW MRI of patient 2 acquired with STEAM (top) and ssEPI (bottom). Left to right, anatomical image, trace-weighted images at b = 50 s mm^{-2} and b = 600 s mm^{-2}, and ADC map. While the STEAM ADC map reveals a lenticular area with low signal intensity in the left transition zone in agreement with T_2-weighted MRI (PI-RADS score = 5), this lesion is less clear in the ssEPI ADC map (arrows)

of the prostate from the peripheral zone, which is not the case for ssEPI. Supplementary Figure 1 shows an additional lesion of Patient 2, which was characterized by an experimental STEAM MRI protocol with b-values up to 1400 s mm^{-2}.

4 | DISCUSSION

This work reports the development and first application of a DW STEAM MRI technique to prostate imaging. The multi-shot method employs rotated radial trajectories and an inverse reconstruction algorithm with denoising of phase maps. Extending previous STEAM variants,[8,9,12] the present method achieves DW MRI of the prostate without the use of an endorectal coil within clinically feasible measuring times. Apart from good spatial resolution, adequate SNR, and accurate ADC values, the diagnostic image quality benefits from the absence of susceptibility-induced geometric distortions and false signal intensities.

The inherent physical properties of STEAM sequences offer several practical advantages for DW MRI of the prostate. First, the method provides access to tissue in the vicinity of the intestinal wall even in cases where susceptibility problems degrade EPI-based acquisitions. This robustness also improves patient compliance, as it removes the necessity for inconvenient preparations such as rectal filling or fasting prior to MRI. Second, although limited to two patients, the present observations suggest that DW STEAM images and ADC maps may lead to a more accurate anatomical delineation of prostate lesions than possible with EPI. Apart from the actual diagnostic value, this property also renders DW STEAM MRI a promising choice for radiotherapy planning in the prostate.[6,7] Third, DW STEAM MRI may enhance diagnostic reliability by eliminating the risk of misinterpretations of susceptibility-induced signal alterations. This problem has previously been reported for DW MRI of the prostate[2] and brain.[20]

Although rsEPI may reduce susceptibility-induced distortions in DW MRI of the prostate compared with ssEPI,[5-7] in this study the artifacts observed with ssEPI were mostly retained with rsEPI. Additionally, ADC values obtained by DW rsEPI largely deviated from those measured with either STEAM or ssEPI. This observation hints at an unstable ADC calculation because of low SNR, possibly due to an adjustment of the in-plane resolution from the default setting of 1.8 × 1.8 mm^2 to 1.4 × 1.4 mm^2 (as for STEAM and ssEPI). Hence, with regard to both SNR efficiency and artifact suppression, multi-shot STEAM MRI emerges as a more promising alternative for clinical prostate DW MRI than the applied rsEPI protocol.

A limitation of the present work is the use of a maximal *b*-value of 600 s mm^{-2}. This was taken as a practical compromise between contrast and SNR of the DW images and was originally optimized for healthy volunteers. However, this choice is also justified from a clinical perspective because Esen et al[21] reported a similar sensitivity and specificity of prostate cancer diagnosis for *b*-values of 600 s mm^{-2} and 1000 s mm^{-2}. Moreover, preliminary results (for Patient 2) demonstrate the technical feasibility of DW STEAM MRI with *b*-values up to 1400 s mm^{-2}. Another obstacle to the proposed technique is the long reconstruction time, which at this stage precludes widespread clinical application. The problem will soon be solved by an implementation of the algorithm on a multi-GPU computer, which has been integrated into the used MRI system. It already allows for nonlinear inverse reconstructions of dynamic image series in real time.[11,22] A third limitation of the present study is its focus on healthy volunteers. This is because the primary aim was a proof-of-principle evaluation of a newly developed DW STEAM MRI method with emphasis on technical feasibility and achievable diagnostic image quality. Having demonstrated clinically relevant benefits in comparison with established EPI-based protocols, the next step must be an assessment of the diagnostic performance of DW STEAM MRI in extended patient studies.

CONFLICTS OF INTEREST

The authors declare no conflict of interest.

FUNDING INFORMATION

Dr Sabine Hofer gratefully acknowledges financial support by the Deutsche Krebshilfe e.V.

ORCID

Andreas Merrem https://orcid.org/0000-0001-5429-4241
Zhengguo Tan https://orcid.org/0000-0002-4322-5109

REFERENCES

1. Torre A, Bray F, Siegel R, et al. Global cancer statistics, 2012. *CA Cancer J Clin*. 2015;65:87-108.
2. Tan C, Wang J, Kundra V. Diffusion weighted imaging in prostate cancer. *Eur Radiol*. 2011;21:593-603.
3. Barentsz J, Reichenberg J, Clements J, et al. ESUR prostate MR guidelines 2012. *Eur Radiol*. 2012;22:746-757.
4. Mansfield P. Multi-planar image formation using NMR spin echoes. *J Phys C*. 1977;10:L55-L58.
5. Li L, Wang L, Deng M, et al. Feasibility study of 3-T DWI of the prostate: readout-segmented versus single-shot echo-planar imaging. *Am J Roentgenol*. 2015;205:70-76.
6. Liney G, Holloway L, Al Harthi T, et al. Quantitative evaluation of diffusion-weighted imaging techniques for the purposes of radiotherapy planning in the prostate. *Br J Radiol*. 2015;88:20150034.
7. Foltz W, Porter D, Simeonov A, et al. Readout-segmented echo-planar diffusion-weighted imaging improves geometric performance for image-guided radiation therapy of pelvic tumors. *Radiother Oncol*. 2015;117:525-531.
8. Nolte UG, Finsterbusch J, Frahm J. Rapid isotropic diffusion mapping without susceptibility artifacts: whole brain studies using diffusion-weighted single-shot STEAM MR imaging. *Magn Reson Med*. 2000;44:731-736.
9. Karaus A, Hofer S, Frahm J. Separation of fiber tracts within the human cingulum bundle using single-shot STEAM DTI. *Open Med Imaging J*. 2009;3:21-27.
10. Zhang Q, Coolen BF, Versluis MJ, Strijkers GJ, Nederveen AJ. Diffusion-prepared stimulated-echo turbo spin echo (DPsti-TSE): an eddy current-insensitive sequence for three-dimensional high-resolution and undistorted diffusion-weighted imaging. *NMR Biomed*. 2017;30. https://doi.org/10.1002/nbm.3719
11. Uecker M, Zhang S, Voit D, Karaus A, Merboldt KD, Frahm J. Real-time MRI at a resolution of 20 ms. *NMR Biomed*. 2010;23:986-994.

12. Merrem A, Hofer S, Voit D, et al. Rapid diffusion-weighted imaging of the brain without susceptibility artifacts: single-shot STEAM with radial undersampling and iterative reconstruction. *Invest Radiol*. 2017;52:428-433.
13. Haase A, Frahm J, Hänicke W, et al. ^{1}H NMR chemical shift selective (CHESS) imaging. *Phys Med Biol*. 1985;30:341-344.
14. Klosowski J, Frahm J. Image denoising for real-time MRI. *Magn Reson Med*. 2016;77:1340-1352.
15. Block KT, Frahm J. Spiral imaging: a critical appraisal. *J Magn Reson Imaging*. 2005;21:657-668.
16. Guerkin-Kern M, Lejeune L, Pruessmann K, Unser M. Realistic analytical phantoms for parallel magnetic resonance imaging. *IEEE Trans Med Imaging*. 2012;31:626-636.
17. Uecker M, Karaus A, Frahm J. Inverse reconstruction method for segmented multishot diffusion-weighted MRI with multiple coils. *Magn Reson Med*. 2009;62:1342-1348.
18. Pickles M, Gibbs P, Sreenivas M, et al. Diffusion-weighted imaging of normal and malignant prostate tissue at 3.0 T. *J Magn Reson Imaging*. 2006;23:130-134.
19. Emad-Eldin S, Halim M, Lamiaa I, et al. Diffusion-weighted MR imaging and ADC measurement in normal prostate, benign prostatic hyperplasia and prostate carcinoma. *Egypt J Radiol Nucl Med*. 2014;45:535-542.
20. Khalil AA, Hohenhaus M, Kunze C, et al. Sensitivity of diffusion-weighted STEAM MRI and EPI-DWI to infratentorial ischemic stroke. *PLoS ONE*. 2016;11:e0161416.
21. Esen M, Onur M, Akpolat N, et al. Utility of ADC measurement on diffusion-weighted MRI in differentiation of prostate cancer, normal prostate, And Prostatitis. *Quant Imaging Med Surg*. 2013;3:210-216.
22. Schaetz S, Voit D, Frahm J, et al. Accelerated computing in magnetic resonance imaging: real-time imaging using nonlinear inverse reconstruction. *Comput Math Methods Med*. 2017;3527269.

SUPPORTING INFORMATION

Additional supporting information may be found online in the Supporting Information section at the end of the article.

How to cite this article: Merrem A, Hofer S, Seif Amir Hosseini A, et al. Diffusion-weighted MRI of the prostate without susceptibility artifacts: Undersampled multi-shot turbo-STEAM with rotated radial trajectories. *NMR in Biomedicine*. 2019;e4074. https://doi.org/10.1002/nbm.4074